Injection into a Rocket Nozzle," AIAA Paper 69-443, Colorado Springs, Colo., 1969.

[15] Crist, S., Sherman, P. M., and Glass, D. R., "Study of the Highly Under-expanded Sonic Jet," *AIAA Journal*, Vol. 4, No. 1, Jan. 1966, pp. 68–71.

[16] Adamson, Jr., T. C. and Nicholls, J. A., "On the Structure of Jets from Highly Underexpanded Nozzles into Still Air," *Journal of the Aerospace Sciences*, Vol. 26, No. 1, 1959, pp. 16–24.

[17] Love, E. S. and Grigsby, C. E., "Some Studies of Axisymmetric Free Jets Exhausting from Sonic and Supersonic Nozzles into Still Air and into Supersonic Streams," RM L54L31, 1955' NACA.

[18] Morkovin, M. V., Pierce, C. A., and Craven, C. E., "Interaction of a Side Jet with a Supersonic Main Stream," Bulletin 35, 1952, Univ. of Michigan, Engineering Research Institute, Ann Arbor, Mich.

[19] Owen, P. L. and Thornhill, C. K., "The Flow in an Axially-Symmetric Supersonic Jet from a Nearly Sonic Orifice into a Vacuum," R and M 2616, 1952, British Aeronautical Research Council.

JUNE 1971 AIAA JOURNAL VOL. 9, NO. 6

Acoustic Characteristics of a High-Subsonic Jet

L. MAESTRELLO* AND E. MCDAID†
NASA Langley Research Center, Hampton, Va.

The acoustic source regions of a subsonic cold jet were traced as far as the periphery of the jet by means of the pressure field on a plane rigid surface located in the vicinity of the jet. The centers of these regions were determined to be from 4 to 18 diam downstream of the exit. Additional measurements were made of flow variables within the jet. From these measurements, the downstream kinetic energy dissipation rate was calculated. Finally, the acoustic radiation characteristics of several simple nozzle configurations were measured. Results indicate that, although considerable alternating of directivity and spectral content of the noise result from varying nozzle geometry, only limited reductions in total sound power resulted.

Introduction

THE general format for nearly all recent work in aerodynamic noise was established by Lighthill[1,2] when he related the sound pressure generated by turbulence to a system of equivalent quadrupole sources in a medium at rest. An alternate approach, mathematically equivalent to Lighthill's but using simple sources, was developed by Ribner.[3] Initial application of the Lighthill theory was made by Proudman,[4] who determined the sound pressure generated by isotropic turbulence. Lilley[5] first used the classification "self noise" and "shear noise" of jets to separate the high-frequency noise due to turbulence-turbulence interaction from the low-frequency noise due to turbulence-shear interaction. The effects of convection were discussed by Ffowcs Williams[6] as well as by Jones.[7] Application of the theory to the radiation of sound in the presence of surfaces was done by Curle,[8] Powell,[9] Lyamshev,[10] and Ffowcs Williams.[11] Acoustic aspects of combustion instability were reported by Kandratiev and Rimski-Korsakov.[12] The distribution of acoustic sources in the jet was determined by Ribner[13] and Powell[14] using similarity considerations and Lighthill's U^8 law. Ribner[15] recently showed that for a low-speed jet, only nine of the possible 36 distinct quadrupole correlations yield distinct nonvanishing contributions to the sound power.

The present paper introduces an experimental technique to locate the acoustic source regions of a jet. In addition, acoustic measurements were made of changes in directivity, spectral content, and total sound power due to changes in nozzle geometry.

Presented as Paper 70-234 at the AIAA 8th Aerospace Sciences Meeting, New York, January 19–21, 1970; submitted February 9, 1970; revision received November 23, 1970. The authors wish to express thanks to J. E. Ffowcs Williams for his helpful discussions and T. Clark for his technical assistance.

* Aero-Space Technologist, Acoustic Branch. Member AIAA.
† Aero-Space Technologist, Acoustic Branch.

Distribution of Sound Sources in a Jet

Lighthill formulated the aerodynamic noise problem using an acoustic analogy. In this model, the fluid turbulence giving rise to sound generation and scattering are replaced by an equivalent distribution of acoustic quadrupole sources in a medium at rest. Mathematically, the model appears as the following nonhomogeneous wave equation

$$\partial^2\rho/\partial t^2 - a_0^2\nabla\rho^2 = \partial^2 T_{ij}/\partial x_i \partial x_j$$

where $T_{ij} = \rho v_i v_j - \tau_{ij} + (p - a_0^2\rho)\delta_{ij}$, a_0^2 is the local speed of sound, ρ is the density, v_i is a component of velocity, τ_{ij} is the viscous stress, and p is the thermodynamic pressure.

In the absence of surfaces, this wave equation can be replaced by the following integral equation for points $\mathbf{x}$ in the far field

$$\Delta\rho(\mathbf{x},t) = \frac{x_i x_j}{4\pi a_0^4 |\mathbf{x}|^3} \int \frac{\partial^2 T_{ij}\mathbf{y}, t - |\mathbf{x} - \mathbf{y}|/a_0}{\partial t^2}\, d^3|\mathbf{y}|$$

where $\Delta\rho(\mathbf{x},t) = \rho(\mathbf{x},t) - \rho_0$, and ρ_0 is the density of the acoustic medium at rest.

The autocorrelation of the far-field density fluctuation can be written as

$$R(\mathbf{x},\tau) = \frac{x_i x_j x_l x_m}{16\pi^2 a_0^8 |\mathbf{x}|^6} \iint \frac{\partial^4}{\partial \tau_0^4} R_{ijlm}(\mathbf{y},\mathbf{y}',\tau_0) d^3|\mathbf{y}| d^3|\mathbf{y}'|$$

where

$$R_{ijlm}(\mathbf{y},\mathbf{y}',\tau_0) = \overline{T_{ij}(\mathbf{y},\tau') T_{lm}(\mathbf{y}',\tau' + \tau_0)}$$

$$\tau' = t - |\mathbf{x} - \mathbf{y}|/a_0,\ \tau_0 = \tau - (|\mathbf{x} - \mathbf{y}'| - |\mathbf{x} - \mathbf{y}|)/a_0$$

Efforts to determine the acoustic source locations in a jet have centered around the determination of the tensor R_{ijlm}.[16]

An alternate approach has been used in the present investigation. Instead of actually measuring R_{ijlm} within the jet, measurements of the sound field near the jet have been

used. Using Kirchoff's solution of the nonhomogeneous wave equation, one can show that a plane rigid surface near a jet acts as a specular reflector for the sound from the quadrupole source distribution in the jet. There is thus a distribution of virtual, acoustic sources induced on the surface. If the surface is sufficiently close to the jet, then the downstream positions of the virtual sources on the plane surface and the quadrupole sources in the jet should correspond to within a certain small number of radii. These ideas are developed below.

In the presence of a rigid surface, the acoustic far field of the jet can be written as[8]

$$\Delta p = \frac{1}{4\pi}\frac{\partial^2}{\partial x_i \partial x_j}\int_v \frac{T_{ij}[\mathbf{y},t-(|\mathbf{x}-\mathbf{y}|/a_0)]}{|\mathbf{x}-\mathbf{y}|}\,d^3|\mathbf{y}| + \frac{1}{4\pi a_0}\int_s \frac{\partial}{\partial n}|\mathbf{x}-\mathbf{y}|\frac{\partial}{\partial t}P\left(\mathbf{y},t-\frac{|\mathbf{x}-\mathbf{y}|}{a_0}\right)\frac{d^2|\mathbf{y}|}{|\mathbf{x}-\mathbf{y}|}$$

Powell[9] shows that this surface integral is equivalent to the sound that would be generated by an image jet beneath the surface. The far-field radiation from the surface is

$$P(\mathbf{x},t) = -\frac{1}{4\pi a_0}\int_s \frac{\partial}{\partial n}|\mathbf{x}-\mathbf{y}|\frac{\partial}{\partial t}p\left(\mathbf{y},t-\frac{|\mathbf{x}-\mathbf{y}|}{a_0}\right)\frac{d^2|\mathbf{y}|}{|\mathbf{x}-\mathbf{y}|}$$

Since the pressure on the plate is significant only over a limited region, the following approximation can be used (Fig. 2):

$$P(\mathbf{x},t) = \frac{\cos\theta}{4\pi|\mathbf{x}|a_0}\int_s \frac{\partial}{\partial t}p\left(y,t-\frac{|\mathbf{x}-\mathbf{y}|}{a_0}\right)d^2|\mathbf{y}|$$

The corresponding pressure correlation at $\mathbf{x}$ is

$$R(\mathbf{x},\tau) = \frac{\cos^2\theta}{16\pi^2 a_0^2 r^2}\int_s\int_s \overline{\frac{\partial}{\partial\tau_1}p(\mathbf{y},\tau_1)\frac{\partial}{\partial\tau_2}p(\mathbf{z},\tau_2)}\,d^2|\mathbf{y}|d^2|\mathbf{z}|$$

where

$$\tau_1 = t-(|\mathbf{x}-\mathbf{y}|/a_0),\ \tau_2 = t+\tau-(|\mathbf{x}-\mathbf{z}|/a_0)$$

Hence,

$$\mathcal{R}(\mathbf{x},\tau) = \frac{\cos^2\theta}{16\pi^2 a_0^2 r^2}\int_s\int_s \frac{\partial^2}{\partial\tau^{*2}}R(\mathbf{y},\mathbf{z},\tau^*)d^2|\mathbf{y}|d^2|\mathbf{z}|$$

with

$$R(\mathbf{y},\mathbf{z},\tau^*) = \overline{p(\mathbf{y},\tau_1)p(\mathbf{z},\tau_1+\tau^*)} \text{ and } \tau^* = \tau_2-\tau_1$$

The power spectral density S, of the pressure at $\mathbf{x}$, is given by the Fourier transform of $\mathcal{R}(\mathbf{x},\tau)$;

$$S(\mathbf{x},\omega) = \frac{\omega^2\cos^2\theta}{16\pi^2 r^2 a_0^2}\iint \exp\left\{-i\frac{\omega|\lambda|}{a_0}\sin\theta\cos[\phi(\mathbf{z})-\phi(\mathbf{y})]\right\}\times R_\omega(\mathbf{y},\mathbf{z})d^2|\mathbf{y}|d^2|\mathbf{z}| \quad (1)$$

where

$$R_\omega(\mathbf{y},\mathbf{z}) = \int_{-\infty}^{\infty} R(\mathbf{y},\mathbf{z},\tau^*)\exp[-i\omega\tau^*]d\tau$$

and $\boldsymbol{\lambda} = \mathbf{z}-\mathbf{y}$ and $|\mathbf{x}-\mathbf{z}|-|\mathbf{x}-\mathbf{y}| \approx |\boldsymbol{\lambda}|\sin\theta\cos[\phi(\mathbf{z})-\phi(\mathbf{y})]$.

Using Eq. (1), a partial radiation source density is defined to be the y-integrand and is interpreted as the contribution to the ω-component of the mean square pressure at point $\mathbf{x}$ contributed by a point $\mathbf{y}$ on the plate

$$d(\mathbf{x},\mathbf{y},\omega) = \frac{\omega^2\cos^2\theta}{16\pi^2 a_0^2 r^2}\int_s \exp\left\{-i\frac{\omega|\lambda|}{a_0}\sin\theta\cos[\phi(\mathbf{z})-\phi(\mathbf{y})]\right\}\times R_\omega(\mathbf{y},\mathbf{z})d^2|\mathbf{z}|$$

Furthermore, the radiation source density for the plate is defined as the integral, over all observation points on a hemisphere (Ω), of $d(\mathbf{x},\mathbf{y},\omega)$:

$$D(\mathbf{y},\omega) = \int_\Omega d(\mathbf{x},\mathbf{y},\omega)d^2|\mathbf{x}|$$

Upon carrying out the integration,[17] the equation becomes

$$D(\mathbf{y},\omega) = \frac{1}{8\pi}\int_s \frac{R_\omega(\mathbf{y},\mathbf{z})}{|\lambda|^2}\left[\frac{\sin\omega|\lambda|/a_0}{\omega|\lambda|/a_0}-\cos\frac{\omega|\lambda|}{a_0}\right]d^2|\mathbf{z}|$$

The function $D(\mathbf{y},\omega)$ is the power spectral density of the acoustic pressure radiated from a unit area at point $\mathbf{y}$ on the surface. It corresponds to a distribution of acoustic sources on the plate. In order to be useful, $D(\mathbf{y},\omega)$ must be related to the sources in the jet. The general function relationship between D and R_{ijlm}, although easily written formally, is quite complicated.

One can refine the estimate of the positions of those regions of the jet giving rise to the virtual source distribution D in the following manner. If the pressure field on the plate is purely acoustic, then it is possible to perform a wave vector decomposition of the field to determine at what angle the sound has impinged upon the surface. Since pressure perturbations in space will, by assumption, thus have phase velocity a_0, the phase velocities of the acoustic pressure fluctuations on the plate will correspond to the directions of propagation of the sound. These directions will yield the regions of the jet from which the noise has emanated. A three-dimensional acoustic pressure wave can be expressed in terms of its wave vector components as the Fourier integral[18]

$$P(\mathbf{r},t) = \frac{1}{8\pi^3}\int_{-\infty}^{\infty}\int_{-\infty}^{\infty}\int_{-\infty}^{\infty}\exp[i(\mathbf{k}\cdot\mathbf{r}-\kappa a_0 t)]dF(\mathbf{k})$$

where $|\mathbf{k}| = \kappa$.

If it is assumed that the pressure field is homogeneous and stationary, the space-time correlation can be written in the form

$$R_0(\boldsymbol{\lambda},\tau) = \frac{1}{8\pi^3}\int_{-\infty}^{\infty}\int_{-\infty}^{\infty}\int_{-\infty}^{\infty} dk_1 dk_2 dk_3 M_0(k_1,k_2,k_3)\times \exp i[\mathbf{k}\cdot\boldsymbol{\lambda}-\kappa\tau a_0]$$

where k_1, k_2, and k_3 are the components of $\mathbf{k}$, and $\boldsymbol{\lambda}$ is the spatial separation vector. Note that

$$\langle p^2(x)\rangle = \frac{1}{8\pi^3}\int_{-\infty}^{\infty}\int_{-\infty}^{\infty}\int_{-\infty}^{\infty} dk_1 dk_2 dk_3 M_0(k_1,k_2,k_3)$$

Since $\langle p^2(x)\rangle$ is proportional to the acoustic intensity, M_0 is equivalent to a partition of the sound energy into components propagating with frequency $\omega = a_0(k_1^2+k_2^2+k_3^2)^{1/2}$ and in the direction, as specified in the coordinates of Fig. 1,

$$r = 1,\ \phi = \tan^{-1}(k_2/k_1),\ \theta = \cos^{-1}(a_0 k_3/\omega)$$

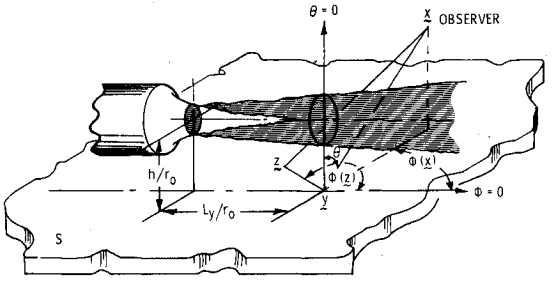

Fig. 1 Geometry for jet image over an infinite, plane, rigid boundary.

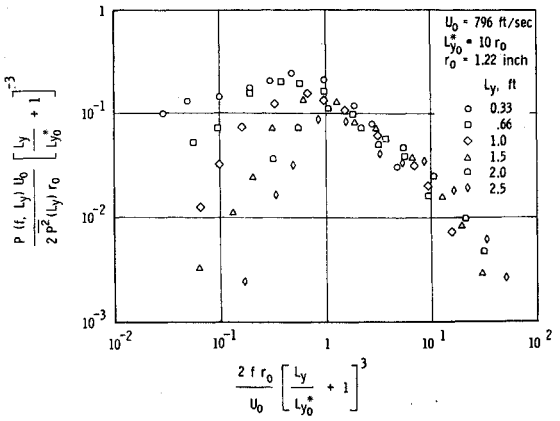

a) Normalized power spectra density of the pressure on the plate

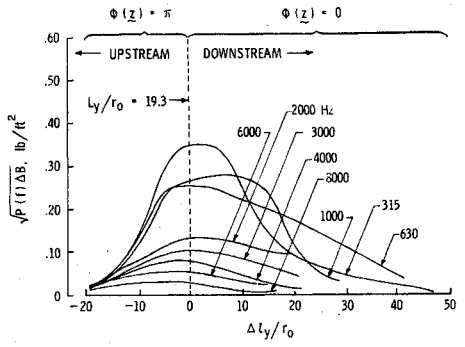

b) Root-mean-square pressure along the jet axis

Fig. 2 Pressure on the plate.

Following Gel'fand and Shilov,[19] the k_3-integration is performed to yield

$$R_{0\omega}(\lambda_1,\lambda_2,0) = \frac{\omega}{4\pi^2 a_0^2}\int_{-\infty}^{\infty}\int_{-\infty}^{\infty} dk_1 dk_2 \times \frac{M_0(k_1,k_2,k_3')\exp[i(k_1\lambda_1 + k_2\lambda_2)]}{k_3'} + \frac{\omega}{4\pi^2 a_0^2}\times \int_{-\infty}^{\infty}\int_{-\infty}^{\infty} dk_1 dk_2 \frac{M_0(k_1,k_2,-k_3')\exp[i(k_1\lambda_1 + k_2\lambda_2)]}{k_3'} \quad (2)$$

where $k_3' = (\omega^2/a_0^2 - k_1^2 - k_2^2)^{1/2}$. Using the notation of Eq. (1) and letting λ_1, λ_2, and λ_3 be the downstream, transverse, and vertical component of $\boldsymbol{\lambda}$, respectively, one has

$$R_\omega(\mathbf{y},\mathbf{y}) = R_{0\omega}(0,0,0) = \frac{\omega}{4\pi^2 a_0^2}\int_{-\infty}^{\infty}\int_{-\infty}^{\infty} dk_1 dk_2 \times \frac{M_0(k_1,k_2,k_3')}{k_3'} + \frac{\omega}{4\pi^2 a_0^2}\int_{-\infty}^{\infty}\int_{-\infty}^{\infty} dk_1 dk_2 \frac{M_0(k_1,k_2,-k_3')}{k_3'}$$

The first term on the right is contributed by the image jet, while the second term is contributed by the real jet. The two integrals are, of course, equal. Thus, one has

$$R_\omega(\mathbf{y},\mathbf{y}+\boldsymbol{\lambda}) = \tfrac{1}{2}R_{0\omega}(\lambda_1,\lambda_2,0) = \frac{\omega}{4\pi^2 a_0^2}\int_{-\infty}^{\infty}\int_{-\infty}^{\infty} dk_1 dk_2 \frac{M_0(k_1,k_2,k_3')\exp[i(k_1\lambda_1 + k_2\lambda_2)]}{k_3'}$$

Letting $N_\omega(k_1,k_2)$ be the Fourier transform of $R_\omega(\mathbf{y},\mathbf{y}+\boldsymbol{\lambda})$ with respect to λ_1 and λ_2, then

$$M_0(k_1,k_2,k_3') = (a_0^2 k_3'/\omega)N_\omega(k_1,k_2) \quad (3)$$

Both experimental and conceptual difficulties arise due to the obvious nonhomogeneity of the sound field over the plate (Fig. 2). The approach used to minimize the effects of the nonhomogeneity is to consider only those frequencies for which the sound field is nearly homogeneous, that is, those for which the sound field may be considered homogeneous over that region of the plate for which $R_\omega(\mathbf{y},\mathbf{y}')$ is nonnegligible.

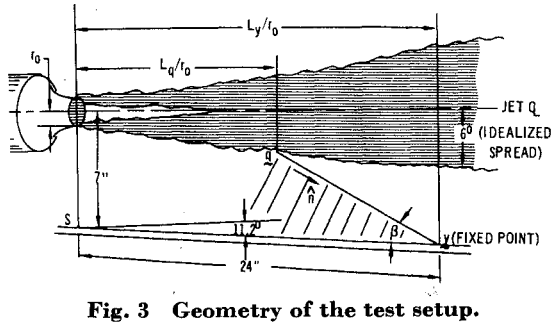

Fig. 3 Geometry of the test setup.

Measurement and Analysis

Location of Acoustic Sources

The evaluation of the integrand $R_\omega(\mathbf{y},\mathbf{z})$ was made by measuring pressure fluctuations over a large rigid plate (Fig. 1) near a cold jet having radius $r_0 = 1.22$ in. The jet exited from a pipe, with a partially turbulent shear exit profile. Upstream of the nozzle exit, an acoustic muffler reduced the flow noise originating in the air supply system to levels well below those generated by the jet itself. The muffler also acted as a settling chamber for the flow. The plate was solidly mounted at a distance $h = 7$ in. from the center of the nozzle at an angle of 11.2° relative to the center line of the jet, Fig. 3. The distance from the plate to the jet was sufficient to eliminate any Coanda effect. Narrow band correlation measurements of the fluctuating pressure were made about a fixed point $\mathbf{y}$, at a position $L_y/r_0 = 19.3$, lying on the projection of the jet center line. The correlations were done along three axes lying on the plate and passing through $\mathbf{y}$. The axes correspond to the rays $\phi = 0$ and π; $\phi = \pi/4$ and $5\pi/4$; and $\phi = \pi/2$ and $3\pi/2$ in Fig. 1. Narrow band correlations were made for eight different center frequencies. A bandwidth of 200 Hz was used for center frequencies of 1000, 2000, 3000, 4000, 6000, and 8000 Hz.

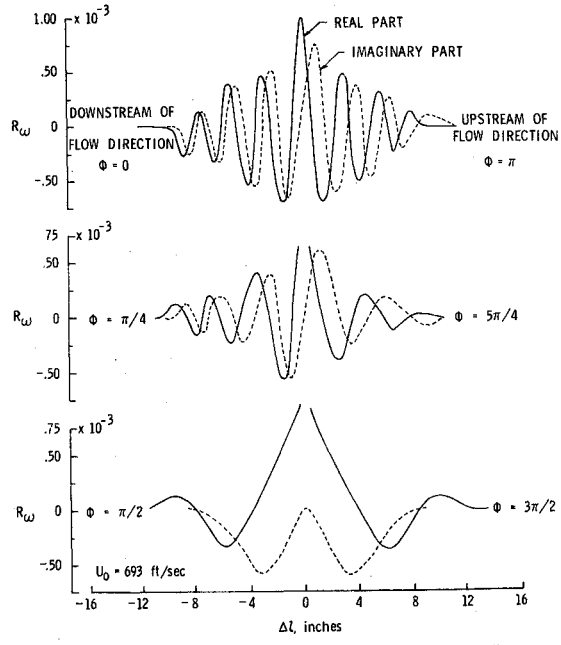

Fig. 4 Typical values of R evaluated along three plate axes at $L_y/r_0 = 19.3$ for 6000 Hz.

Bandwidths of 148 Hz and 74 Hz were used for center frequencies of 630 Hz and 315 Hz, respectively. Pressures were measured using Bruel and Kjaer 0.25-in.-diam condenser microphones mounted flush with the surface. The normalized power spectra of the pressure over the rigid plate are shown in Fig. 2.

The power spectral density of the pressure on the plate is normalized with the local Strouhal number $(2fr_0)/U_0[(L_y)/(L_{y0}) + 1]^3$ obtained from continuity considerations along the jet axis, ignoring the effects of induced flow. U_0 is the mean exit velocity; f is the frequency; L_{y0}‡ is the virtual origin of the flow; L_y is the distance from the nozzle exit to the projection of $\mathbf{y}$ on the jet axis (Fig. 3); $\overline{p^2}$ is the mean square acoustic pressure at L_y; and $P(f,L_y)$ is the power spectral density of the pressure. For those test points incorporated in the figure, the nondimensional power spectral densities collapse with a minimum of scatter of Strouhal numbers greater than 1.0, whereas for low Strouhal numbers, the spread increases. There is evidence of a slight contribution to the pressure on the plate due to induced flow; however, this effect is small and limited to very low frequencies. It is well known that the low frequencies do not scale as well as the higher frequencies.

The distribution of the approximate root-mean-square pressure within the experimental frequency bands $[P(f)\Delta B]^{1/2}$, is shown for eight different center frequencies in Fig. 2. This pressure is shown as a function of position on the plate. These points lie along the projection of the jet axis on the plate. It is clearly evident that the sound field is nonhomogeneous, the nonhomogeneity being apparently greatest for the low frequencies.

Typical measurements of the narrow band spatial correlations are shown in Fig. 4. Measurements made along the axes $\phi = 0, \pi$; $\phi = \pi/4, 5\pi/4$; and $\phi = \pi/2, 3\pi/2$ were used to define $R_\omega(\mathbf{y},\mathbf{z})$ for all points z on the plate. For high frequencies, these measurements allowed R_ω to be defined with sufficient accuracy; whereas for the lower frequencies, additional test points on a greater number of axes would be desirable.

The wave-vector spectrum from Eq. (3) is shown in Fig. 5 for five different values of k_2. The function is symmetric in k_2. It displays a pronounced maximum on the k_1 axis, which corresponds to sound propagating downstream.

The interpretation of wave-vector spectra in terms of source positions must be done with some caution, as will be illustrated by the following example. Consider the case of the sound impinging on the plate, at a frequency of 6000 Hz. The maximum acoustic intensity on the plate, for this particular frequency, occurs at $L_q/r_o \approx 19$. Various regions of the jet have contributed to this intensity, and it is desirable to determine the region contributing most. Using the wave-vector spectrum, it is necessary to assume that, over the interval in which the narrow band correlation is nonnegligible, the spectrum does not change. For the case of the 6000 Hz sound, this interval is about 9 diam long, centered at $L_q/r_o =$ 10. The source region contributing maximally, traced as far as the jet periphery, thus stretches from about 2 to 8 diam from the jet exit. For each test frequency, the table shows the phase velocity c_f, the angle of impingement β, and the downstream position of the center of the source region Lq/r_0 (Fig. 3).

Table 1 Center of source regions from fixed point on plate at $Ly/r_0 = 19.3$

f, Hz	c_f, fps	(β_0)	Lq/r_0
2000	2400	61	17
3000	1262	23	8
4000	1250	22	8
6000	1316	27	10
8000	1280	25	9

‡ The virtual origin used to nondimensionalize the pressure on the plate was assumed to be $-10\ r_0$. Subsequent measurement of the velocity field of the jet, however, indicated a virtual origin of $-2r_0$ for $U_0 = 693$ fps.

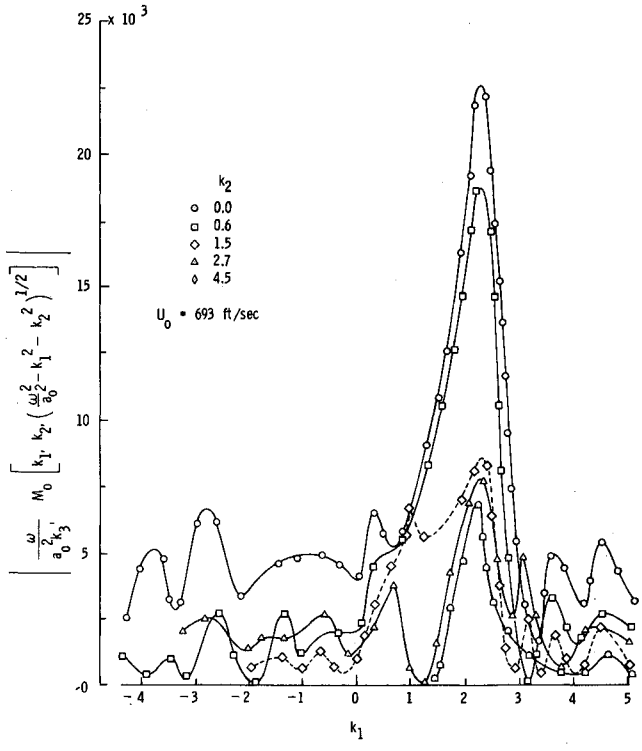

Fig. 5 Typical wave-vector spectrum for frequency 6000 Hz.

The calculated virtual acoustic source density $D(\mathbf{y},\omega)$ is plotted in Fig. 6 for seven different center frequencies, at one point on the plate. The high-frequency dependence of this function is the same as that of the far-field noise of the jet. This indicates that a unit area of the plate is sensitive to a fairly extended region of the jet. Were this not the case, one would expect a high-frequency roll off faster than $1/\omega^2$.

Dynamics of a Freejet

The flowfield of a freejet is characterized by downstream spreading, the entrainment of ambient fluid, viscous dissipation of energy, and acoustic radiation. Measurements of

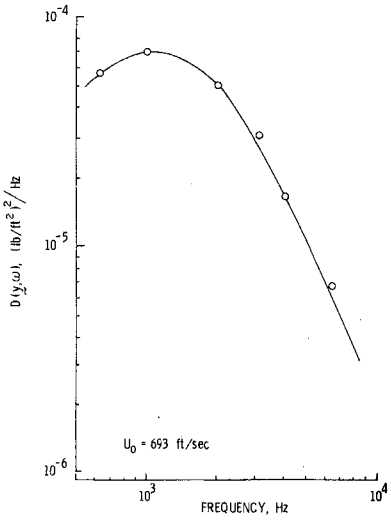

Fig. 6 Radiation source density at $L_y/r_0 = 19.3$.

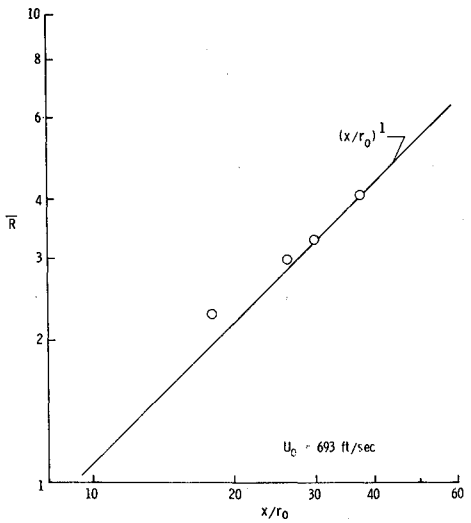

Fig. 7 Mean interface position.

some of these quantities were made for the purpose of relating them to the acoustic sources in the jet.

The effect of entrainment is to increase the flow of fluid across stations downstream of the exit over the initial mass flow issuing from the nozzle itself. The momentum flux, on the other hand, remains constant, and the kinetic energy flux decreases in the downstream direction. The respective definitions of these quantities are given below for a given station x_1, together with simplifying assumptions made for experimental convenience;

mass flow:

$$W(x_1) = \lim_{R\to\infty} \int \rho U(x_1) dS \tag{4}$$

momentum flux:

$$B(x_1) = \lim_{R\to\infty} \int (\rho_0 U^2 + \rho v_1'^2) dS \tag{5}$$

where U and v_i' denote the mean and fluctuating velocities, and ρ_0 is the mean density; the approximations

$$\langle \rho v_1' \rangle \approx 0 \text{ and } \langle \rho v_1'^2 \rangle \approx \rho_0 \langle v_1'^2 \rangle$$

are used.

Kinetic energy flux is

$$E(x_1) = \lim_{R\to\infty} 1/2 \int \rho_0 [U^3 + U \langle 3v_1'^2 + v_1'^2 + v_3'^2 \rangle] dS \tag{6}$$

with approximations

$$\langle \rho v_1'^1 \rangle \approx 0, \langle \rho(v_1'^2 + v_2'^2 + v_3'^2) \rangle \approx \rho_0 \langle v_1^2 + v_2'^2 + v_3'^2 \rangle$$

$$\langle \rho v_1'^2 \rangle \approx \rho_0 \langle v_1'^2 \rangle, \text{ and } \langle \rho v_1' (v_2'^2 + v_2'^2 + v_3'^2) \rangle \approx 0$$

Complete development of these expressions is given in Ref. 20.

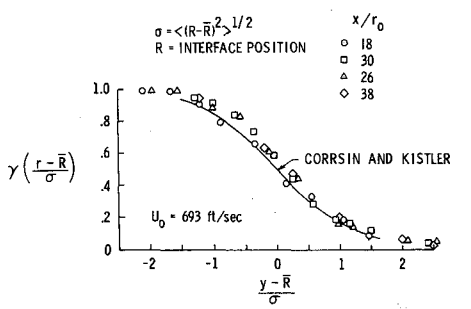

Fig. 8 Intermittency factor $\gamma[(r - \bar{R})/\sigma]$.

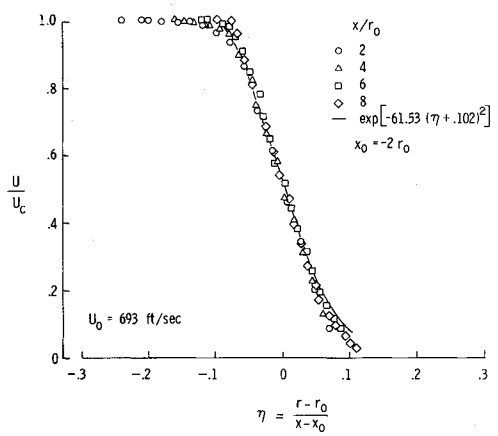

Fig. 9 Universal velocity profile in the mixing region.

The flowfield of the jet has an interface separating the turbulence from the irrotational flow in the surrounding medium. The effect of this fluctuating interface is to introduce an intermittence in the signal from the hot-wire anemometer used to measure the turbulence.

The proportion of the time that a point is within the turbulent region of the jet is termed the intermittency factor γ. Estimates of the properties of the flowfield based on measurements must allow for this intermittency.[21]

The radial and longitudinal distributions of the mean velocity were measured with a constant-temperature hot-wire anemometer. Measurements of the static pressure were made with a standard static pressure tube (0.062-in.-diam) mounted on a turntable to reduce the error in yaw and pitch. The turbulent intensity was measured with a dual-channel, linearized, constant-temperature anemometer using a cross-wire calibrated for yaw angle and cooling.

The signal used to discriminate between the turbulent and nonturbulent regions of the jet was $|\partial^2 v(t)/\partial t^2|$. The differentiation eliminates the low-frequency fluctuations associated with the potential flow outside the turbulent region. The signal was then processed in a standard manner to yield γ.

Figure 7 shows the mean position of the interface for several stations downstream of the nozzle. In Fig. 8 are shown normalized intermittency values which are compared with results of Corrsin and Kistler.[22]

A round jet, with a partially turbulent exit profile shows two downstream regions in which the flow profile deforms in a self-similar fashion. One of these regions is the mixing region from $x/r_0 = 2$ to $x/r_0 = 8$. The other region of similarity corresponds to the transition and fully turbulent regions for $x/r_0 > 10$.

The similarity relationship in the mixing region, shown in Fig. 9, is given by the equation

$$U/U_c = \exp[-61.53(\eta + 0.102)^2] \tag{7}$$

where $\eta = (r - r_0)/(x - x_0)$, and the virtual origin $x_0 = -2r_0$.

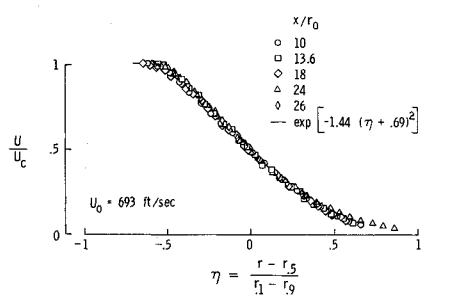

Fig. 10 Universal velocity profile in the transition and partially turbulent regions.

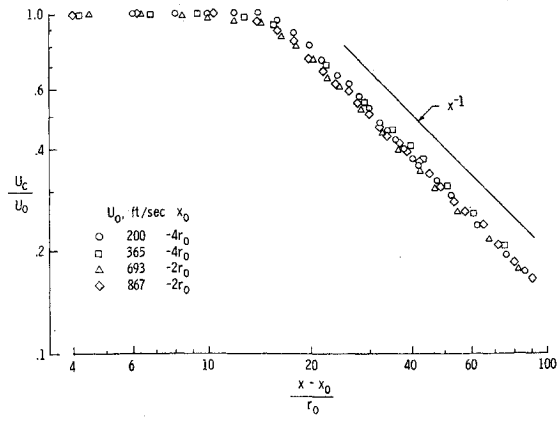

Fig. 11 Distribution of center-line velocities.

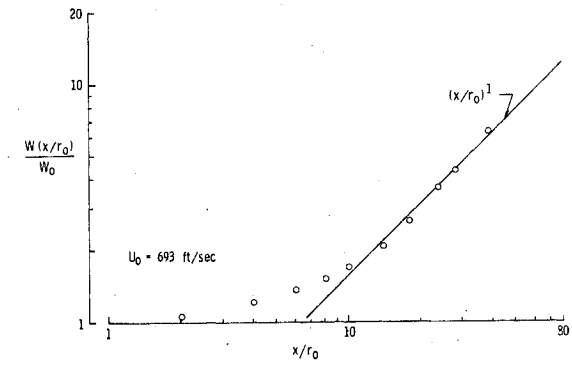

Fig. 13 Mass flow distribution along the jet.

In the transition region, the similarity relationship (Fig. 10) is defined by the equation

$$U/U_c = \exp[-1.44(\eta + 0.69)^2] \quad (8)$$

where $\eta = (r - r_{0.5})/(r_{0.1} - r_{0.9})$, and $r_{0.1}$, $r_{0.5}$, $r_{0.9}$ are those radii when U/U_c is 0.1, 0.5, and 0.9, respectively.

For the range of x/r_0 shown, Eqs. (7) and (8) fit the data fairly well. The virtual origin in Eq. (7) was obtained by extrapolation of the difference $r_{0.1} - r_{0.9}$ to zero. None of the data have yet been corrected for the effects of intermittency. The values of the parameters appearing in Eq. (8) are in close agreement with those found by Nyar et al.[23]

The distribution of jet center-line velocity is shown in Fig. 11 for four different exit center-line velocities. There are two distinct regions of similar behavior. Close to the nozzle, the ratio of U_c/U_o falls off as the inverse of x/r_0. The normalization used in Fig. 11 depends upon the virtual origin of the fully developed region of the jet, which varies with U0. Similar distributions have been reported by Laufer.[24]

Figure 12 shows the distribution of the pressure coefficient $\Delta P/\rho U_c^2$, along the center line. Measurements of the static pressure are influenced by the interaction between the probe and the unsteady velocity field. The measurement of this pressure has been the subject of much argument in the past. A method of measurement similar to that of Bradbury[25] and Toomre[26] has been adopted for this test. The static pressure measured by the probe is defined as $P_s = p + 1/2\rho n(\langle v_R'^2\rangle + \langle v_1'^2\rangle)$, where n is a constant determined by the experiment in terms of scale/probe size. The pressure coefficient is then defined as

$$\frac{P_s - P_a}{\rho U_c^2} = -\frac{\langle v_R'^2\rangle}{U^2} + \frac{1}{2}\,n\left(\frac{\langle v_R'^2\rangle}{U_c^2} + \frac{\langle v_1'^2\rangle}{U_c^2}\right)$$

where v_R' and v_1' are the radial and axial components of turbulence, respectively. For larger values of x/r_0, the pressure coefficient becomes constant indicating self-preservation of the turbulence.

Measurements of the mass flow are shown in Fig. 13. The rate of entrainment is seen to increase until it reaches an apparent constant value at about $x/r_0 = 30$.

The kinetic energy flux of the jet, plotted as a ratio with respect to the kinetic energy flux at the nozzle exit, is shown in Fig. 14. The rate of decrease of kinetic energy flux along the jet axis, obtained from a curve which fits the data of Fig. 14, is shown in Fig. 15. The kinetic energy is seen to fall off rapidly at a constant rate for the first 10 radii downstream.

The total loss in this length is about 35%. This result is consistent with that of Albertson et al.[27] Farther downstream the rate of decrease drops sharply and varies approximately as $(x/r_0)^{-2}$. These experimental results have not been corrected for the effects of intermittency.

Correction for the effects of intermittency would yield the result (Kibens[28])

$$E = \lim_{R\to\infty} \int_s \tfrac{1}{2}\gamma\langle\rho v_T^2 \mathbf{v}_T\rangle ds + \lim_{R\to\infty} \int_s \tfrac{1}{2}(1-\gamma)\langle\rho v_p^2 \mathbf{v}_p\rangle \mathbf{ds}$$

where v_T and v_p are the instantaneous velocities in the turbulence and potential flow, respectively.

Similarity considerations can be used to arrive at a relationship between the rate of decrease of kinetic energy along the jet and the distribution of acoustic sources. Measurements of the flowfield have shown that there are two distinct regions of similarity for the jet being studied. One region corresponds to the mixing region from the exit to 10 radii downstream; the other corresponds to the fully developed jet beyond 10 radii. For the fully developed jet, the rate of decrease of the energy flux varies as $(x - x_0)^{-2}$, where x_0 is the virtual origin of that region. Lighthill has shown that the acoustic efficiency varies as M^5. Since the local Mach number varies as $(x - x_0)^{-1}$, the local acoustic efficiency varies as $(x - x_0)^{-5}$. The axial distribution of sources

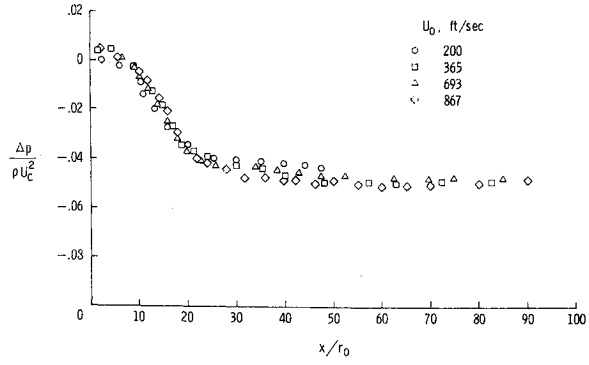

Fig. 12 Distribution of center-line pressure coefficient.

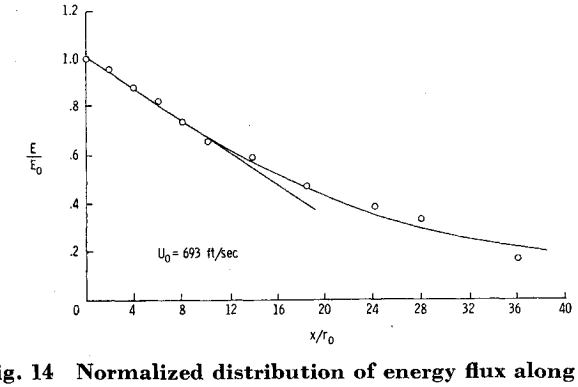

Fig. 14 Normalized distribution of energy flux along the jet.

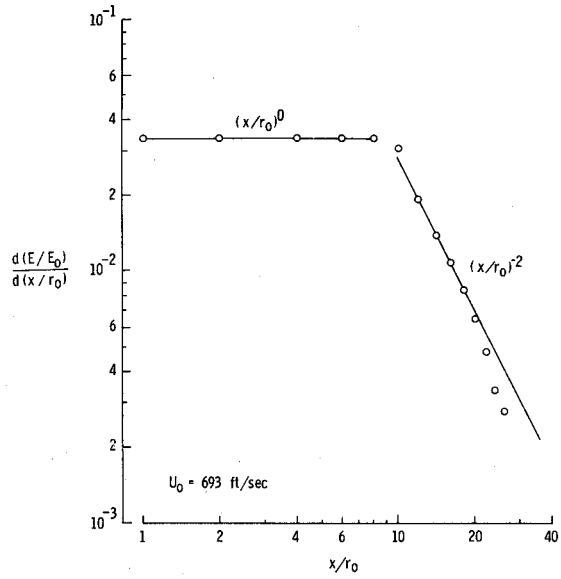

Fig. 15 Normalized distribution of the rate of dissipation of kinetic energy along the jet.

$Q(x/r_0)$ must thus vary as $(x - x_0)^{-7}$, a result consistent with that obtained by Ribner.[18]

In the mixing region, the rate of decrease of energy flux is a constant and the local Mach number is a constant. Thus the distribution of sources $Q(x/r_0)$ must be constant in the region. This is again consistent with Ribner's result.

Engineering Aspects of Jet Noise Reduction

Progress in the development of nozzle suppressors has proceeded largely by empiricism guided to a certain extent by Lighthill's basic theory. Lighthill was able to determine the dependence of the total acoustic power on gross flow parameters such as the mean exit velocity, without detailed knowledge of the turbulent stresses. The usual approach has been to modify a cylindrical nozzle into a suppressor configuration such as the Boeing multitube nozzle. Comparing these two nozzles at constant areas and momenta, one finds that they will have different flow profiles initially, but farther downstream they become increasingly alike. The two jets will radiate nearly the same acoustic power from the region in which they are similar, hence the suppression produced by one of them arises from differences in the initial stages of development of the flowfields.

Presented here are the results of experiments conducted to establish the dependence of the sound field on nozzle geometry, flow velocity profile, and temperature profile. Some of these results have been obtained and discussed

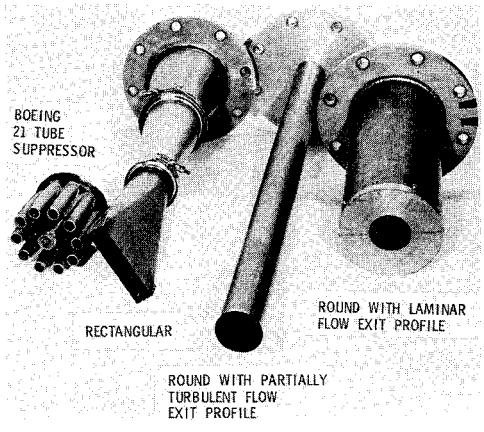

Fig. 16 Nozzle configuration.

Table 2 Behavior of the flowfield of a jet; rotational flow regions

	Mixing region	Fully turbulent region
Uc/U_0	$(x/r_0)^0$	$[(x - x_0)/r_0]^{-1}$
U/Uc	$\exp - 61.53(\eta + 0.102)^2$	$\exp - [1.44(\eta + 0.69)^2]$
$\frac{\Delta P}{\rho Uc^2}$	Decreasing from 0 to -0.045	Constant at -0.045
$\bar{R}$	...	$(x/r_0)^1$
E/E_0	Decreases at a constant rate from 1.0 to 0.65	$(x/r_0)^{-1}$
$\frac{d(E/E_0)}{d(x/r_0)}$	$-(x/r_0)^0$	$-(x/r_0)^{-2}$
$\frac{W(x/r_0)}{W_0}$	Slightly increasing	$(x/r_0)^1$
$Q(x/r_0)$	$(x/r_0)^0$	$(x/r_0)^{-7}$
	Irrotational flow region (ambient fluid)	
V_{radial}	$(r)^{-1}$	
U_1	$(r)^{-\alpha}$ where $\alpha \geqq 2$	
$\overline{u_1^2}$; $\overline{u_2^2}$; $\overline{u_3^2}$	$(r)^{-4}$ (Phillips[29])	

earlier by such investigators as Lassiter and Hubbard,[30] Powell,[31] Lilley,[5] Tyler, Soffrin and Davis,[32] Howes,[33] Mollo-Christensen et al.,[34] and Krishhappa and Csanady.[35]

Acoustic measurements were made in a free field utilizing both the NASA-Langley anechoic chamber facility and the Boeing jet facility. Microphones were positioned at 15° intervals between the angles of 15° and 165° from the jet axis, on a 12-ft radius. Three different sets of microphones were used to insure both adequate sensitivity and frequency response throughout the range of velocities of interest. The configurations tested are shown in Fig. 16. Figure 17 shows the effect on total power radiated, of nozzle geometry and velocity profile. The three nozzles compared have the same

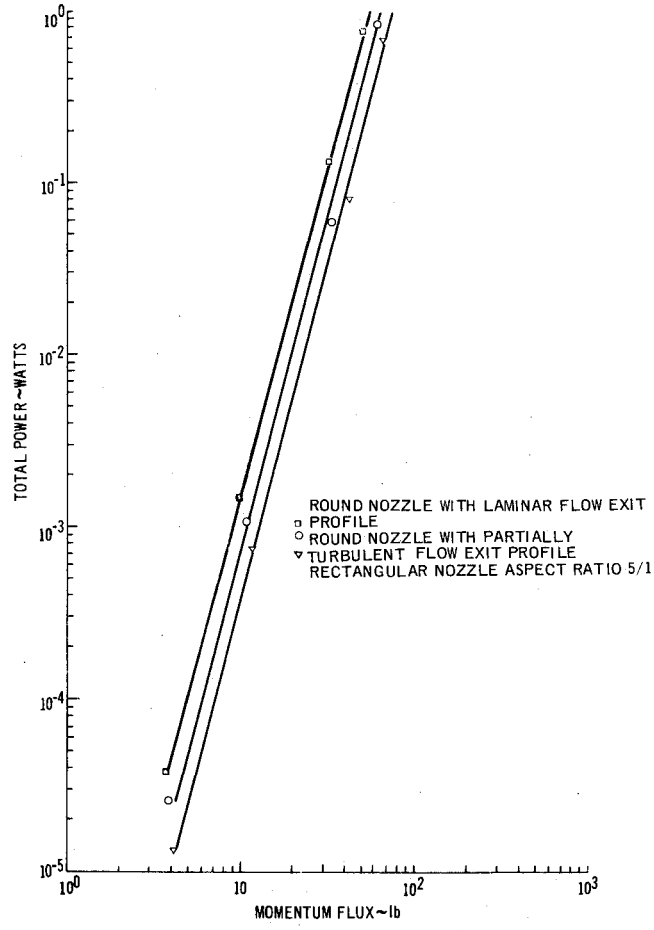

Fig. 17 Effects of nozzle geometry and flow profile on the total acoustic power by a jet of constant area.

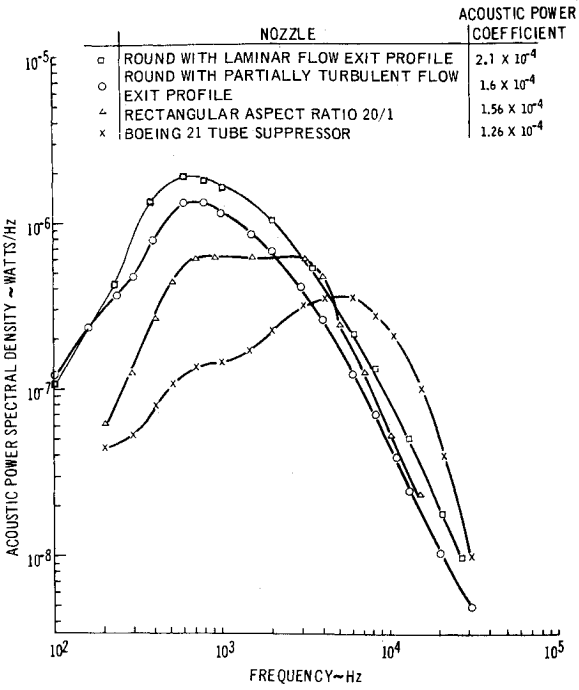

Fig. 18 Effects of nozzle geometry and flow profile on the radiated acoustic power by a jet of constant area and constant flow momentum.

area, 0.032 ft². All nozzles show the expected variation of total acoustic power with the fourth power of thrust. The round nozzle with laminar profile is seen to be a more efficient noise generator than the round nozzle having a partially turbulent profile and the rectangular nozzle with an aspect ratio of 5:1. Powell[31] has shown that if the velocity profile of a jet from a round nozzle is modified further into a parabola, the increase in center-line velocity necessary to maintain a given thrust is sufficient to increase the sound production to a level above that produced by the nozzle with the laminar profile. Figure 18 shows the total acoustic power spectral densities of four different nozzle configurations, all having the same area of 0.0324 ft² and a constant thrust of 48.6 lb. Evaluation of the acoustic power coefficient, defined to be

$$K = \text{acoustic power}/(\rho U^8 A/a_0^5)$$

is also shown in Fig. 18. Of the four nozzles shown, the round nozzle with a laminar flow profile has the highest acoustic power coefficient. The Boeing 21-tube suppressor has the lowest acoustic power coefficient of those nozzles

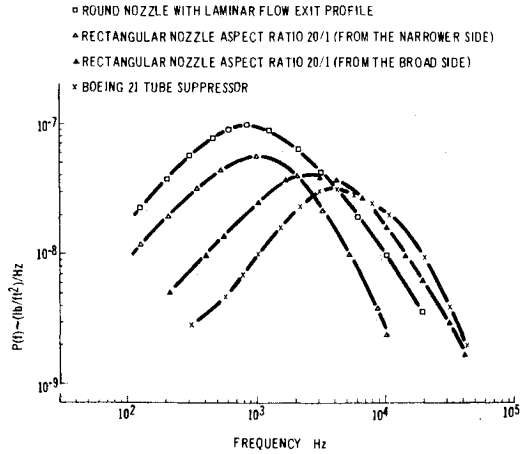

Fig. 19 Power spectral of the sound pressure from 12 ft radius at 45° axis from nozzles at constant area and flow momentum.

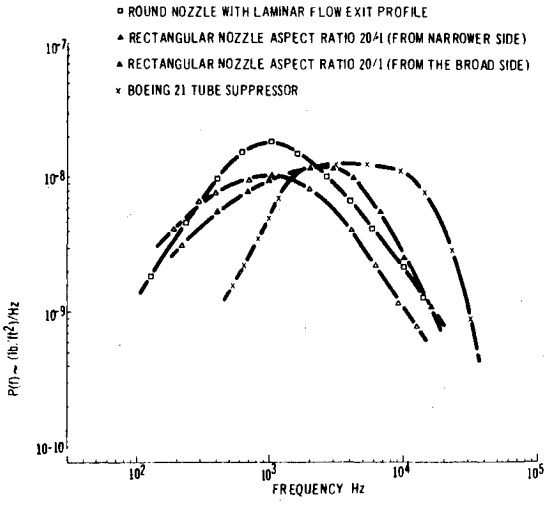

Fig. 20 Power spectral density of sound pressure from 12 ft radius at 90° from jet axis from nozzles at constant area and flow momentum.

tested. It is, however, only slightly better than the rectangular nozzle with an aspect ratio of 20:1.

The acoustic power coefficient is not alone an adequate index of desirable sound generation characteristics of a nozzle. Nozzle geometry affects both the directivity of the sound field and the spectral content of the sound. These aspects of the acoustic radiation are important in such considerations as subjective response to aircraft noise. Directional characteristics of four nozzles are compared in Figs. 19 and 20, at angles of 45° and 90° from the jet axis, respectively. At an angle of 45°, the sound field for the Boeing 21-tube suppressor reaches a maximum which is a factor of 3 lower than the maximum for the standard nozzle; but the maximum for the suppressor occurs at a frequency nearly eight times that at which the maximum of the standard nozzle occurs. For the rectangular nozzle, the maxima opposite the two different sides show a difference by a factor of 2–3, with the sound field opposite the broad side generally of a higher frequency than that opposite the narrow side. The sound fields for the nozzles at 90° from the jet axis are similar in amplitude but show significant differences in spectral content.

It is apparent from the above results that only a limited reduction in total acoustic power is possible by modifying a round nozzle into a suppressor configuration. From this standpoint, the Boeing 21-tube suppressor achieves a reasonable amount of suppression. Further reduction of observed sound generation by a nozzle can be obtained by altering the directional pattern of the sound field as well as the spectral content. This can be realized by varying both the geometry of the nozzle and the temperature distribution at the exit.

References

[1] Lighthill, M. J., "On Sound Generated Aerodynamically, I. General Theory," *Proceedings of the Royal Society*, A211, 1952, pp. 564–587.

[2] Lighthill, M. J., "On Sound Generated Aerodynamically, II. Turbulence as a Source of Sound," *Proceedings of the Royal Society*, A222, 1954, pp. 1–32.

[3] Ribner, H. S., "Aerodynamic Sound From Fluid Dilatations," Rept. 86, 1952, Inst. of Aerophysics Univ. of Toronto, Toronto, Ontario.

[4] Proudman, I., "The Generation of Noise by Isotropic Turbulence," *Proceedings of the Royal Society*, A214, 1952, pp. 119–132.

[5] Lilley, G. M., "On the Noise From Air Jets," Rept. 20, 376-N40-FM2724, 1958, Aeronautical Research Council.

[6] Ffowcs Williams, J. E., "The Noise From Turbulence Convected at High Speed," *Philosophical Transactions*, A255, 1963, pp. 469–503.

[7] Jones, I. S. F., "Aerodynamic Noise Dependent on Mean Shear," *Journal of Fluid Mechanics*, Pt. I, Vol. 33, 1968, pp. 65–72.

[8] Curle, N., "The Influence of Solid Boundaries Upon Aerodynamic Sound," *Proceedings of the Royal Society*, A231, 1955, pp. 505–514.

[9] Powell, A., "Aerodynamic Noise and the Plane Boundary," *Journal of the Acoustical Society of America*, Vol. 31, No. 8, 1960, pp. 982–990.

[10] Lyamshev, L. M., "Analysis of Acoustic Radiation From a Turbulent Aerodynamic Flow," *Soviet Physics-Acoustics*, Vol. 6, No. 4, 1961.

[11] Ffowcs Williams, J. E., "Sound Radiation From a Turbulent Boundary Layer Formed on Compliant Surfaces," *Journal of Fluid Mechanics*, Part II, Vol. 22, 1965, pp. 347–358.

[12] Kandratiev, V. I. and Rimski-Korsakov, A. V., "Instability of Combustion of Intersecting Oxygen and Fuel Jets," 5e Congress Internationale d'acoustic, Liege L56, 1965.

[13] Ribner, H. S., "On the Strength Distribution of Noise Sources Along a Jet," Rept. 51, 1958, Inst. of Aerophysics, Univ. of Toronto, Toronto, Ontario.

[14] Powell, A., "Similarity and Turbulent Jet Noise," *Journal of the Acoustical Society of America*, Vol. 31, No. 6, 1959, pp. 812–813.

[15] Ribner, H. S., "Quadrupole Correlations Governing the Pattern of Jet Noise," *Journal of Fluid Mechanics*, Pt. 1, Vol. 38, 1969, pp. 1–24.

[16] Chu, W. T., "Turbulence Measurements Relevant to Jet Noise," UTIAS Rept. 119, 1966, Univ. of Toronto, Toronto, Ontario.

[17] Maestrello, L. and McDaid, E. P., "Acoustic Characteristics of a High Subsonic Jet," Document D6-24495, April 1970, The Boeing Co., Seattle, Wash.

[18] Morse, P. M. and Feshbach, H., *Method of Theoretical Physics*, McGraw-Hill, New York, 1953, p. 1432.

[19] Gel'fand, I. M. and Shilov, G. E., *Generalized Functions*, Academic Press, New York, 1964, p. 186.

[20] Maestrello, L., "Radiation From and Panel Response to a Supersonic Turbulent Boundary Layer," *Journal of Sound Vibrations*, Vol. 10, No. 2, 1969, pp. 261–295.

[21] Townsend, A. A., *The Structure of Turbulent Shear Flow*, Cambridge University Press, 1956.

[22] Corrsin, S. and Kistler, A. L., "Free-Stream Boundaries of Turbulent Flow," Rept. 1244, 1954, NACA.

[23] Nyar, B. M., Siddon, T. E., and Chu, W. T., "Properties of the Turbulence in the Transition Region of a Round Jet," UTIAS TN 131, 1968, Univ. of Toronto, Toronto, Ontario.

[24] Laufer, J., "On Turbulent Shear Flows of Variable Density," *AIAA Journal*, Vol. 7, No. 4, April 1969, pp. 706–713.

[25] Bradbury, L. J., "The Structure of a Self-Preserving Turbulent Plane Jet," *Journal of Fluid Mechanics*, Vol. 23, 1965, pp. 31–64.

[26] Toomre, A., "The Effect of Turbulence on Static Pressure Measurements," Rept. 22, 010, 1960, Aeronautical Research Council.

[27] Albertson, M. L., Dai, J. A. Y. B., Jensen, R. A., and Rouse, H., "Diffusion of Submerged Jets," Paper 2409, 1948, American Society of Civil Engineers.

[28] Kibens, V., "The Intermittent Region of a Turbulent Boundary Layer," Ph. D. dissertation, 1968, Johns Hopkins Univ., Baltimore, Md.

[29] Phillips, O. M., "The Irrotational Motion Outside a Free Turbulent Jet," *Proceedings of Combined Philosophical Society*, Vol. 51, 1955, pp. 220–229.

[30] Lassiter, L. W. and Hubbard, H. H., "Experimental Studies of Noise From Subsonic Jets in Still Air," TN 2757, 1952, NACA.

[31] Powell, L., "The Influence of the Exit Velocity Profile on the Noise of a Jet," *The Aeronautical Quarterly*, Vol. IV, 1954.

[32] Tyler, J. M., Sofrin, T. G., and Davis, J. W., "Rectangular Nozzles for Jet Noise Suppression," paper presented at the SAE National Aeronautic Meeting, New York, 1959.

[33] Howes, W. L., "Similarity of Far Noise Fields of Jets," TR R-52, 1960, NASA.

[34] Mollo-Christensen, E. and Narashimha, R., "Sound Emission From Jets at High Subsonic Velocities," *Journal of Fluid Mechanics*, Vol. 8, 1960, pp. 49–60.

[35] Krishnappa, G. and Csanady, G. T., "An Experimental Investigation of the Composition of Jet Noise," *Journal of Fluid Mechanics*, Vol. 37, 1969, pp. 149–159.